CrystEngComm

ROYAL SOCIETY OF CHEMISTRY

PAPER

View Article Online
View Journal | View Issue

Cite this: *CrystEngComm*, 2024, **26**, 388

Localization effect for doping and collaborative diffusion in Er^{3+}:YAG melt†

Feng Liu, [a] Xianjie Zhang,[b] Kunfeng Chen, [c] Chao Peng,[a] Guilin Zhuang [b] and Dongfeng Xue *[a]

Received 29th October 2023,
Accepted 12th December 2023

DOI: 10.1039/d3ce01081c

rsc.li/crystengcomm

Coordination geometry variations of cations in yttrium aluminium garnet (YAG) melt system doped with various Er^{3+} concentrations were quantitatively simulated at the classical molecular dynamic level. Our calculated radial distribution functions were discussed upon different ionic pairs, mean square displacement, and diffusion coefficient of ions, on which we clarified two important aspects, namely structure and dynamic properties in YAG melts with intermediate-range order (IRO). Our results show that Er^{3+} doping affects microscopic dynamic melt structures only in a confined scale localizing in the first nearest neighbour of Er^{3+} and O^{2-}. Furthermore, such a localization effect is not varied with Er^{3+} concentration and system temperature. In the present melt system, Y^{3+}, Al^{3+}, and Er^{3+} cations with intrinsic differences (such as mass and electronegativity scales) were found to follow the same diffusion process in this system, which is mainly caused by the wholly collective rearrangement of the network-forming structure. In this Er^{3+}:YAG melt system, there is an equivalence within both structure and dynamics for Er^{3+} and Y^{3+}, which cannot be affected by the system temperature and Er^{3+} concentration, ascribing to the origin of the segregation coefficient of Er^{3+} in YAG to be equal to 1.

Introduction

Yttrium aluminum garnet (YAG, $Y_3Al_5O_{12}$), which has a wide optical transparency, low internal stress, high hardness, chemical resistance, and heat resistance, and lacking birefringence (unlike sapphire),[1–3] is a valuable material for high-energy/high-power laser systems,[4] phosphors,[5] and scintillation materials.[6]

The melt method, such as the Czochralski method, is commonly used to grow YAG single crystals. In order to obtain high-quality YAG crystals by controlling the crystallization kinetics process, YAG melt has attracted the attention of scientists.[7–11] At the micro-scale, the effect of temperature on the bond length between cations and anions is very small.[7,11,12] Under the subcooled state, the bond lengths of Al–O and Y–O in the melts are shorter than those in the crystal,[7] and the situation above the melting point is the same.[11] The coordination numbers both of Al^{3+} and Y^{3+} in the melts are lower than those in the crystal.[11–13] Actually, the decrease in the coordination number is related to the change in the cation coordination structure after melting. In the melted YAG, there are various AlO_n coordination structures, such as AlO_3 (3.6%), AlO_4 (65%), and AlO_5 (28.2%),[13] and there is not only the YO_6 coordination structure but also other coordination structures, such as YO_5 (12.8%), YO_6 (36.6%), YO_7 (34.4%), and YO_8 (13.7%).[13] Our recent simulation results also have demonstrated that indeed there are various cation coordination structures.[14] It is more important that the connected mode between the cation coordination structure has a significant impact on the phase transition or the state of the melt. Due to the similarity between the local structure of the cationic polyhedral connections in the YAG melt and that in YAP ($YAlO_3$), the YAP phase appears during the cooling process in YAG melt,[9,14] which will bring out the inclusions in the YAG crystals and reduce the quality of the crystal. Similarly, the connection between cations can affect the properties of the melt. For example, in the Y_2O_3–Al_2O_3 system, the connection mode of the Y^{3+} polyhedron can induce liquid–liquid phase transitions between low-density and high-density melts.[15–17]

Because pure YAG cannot be used as a working medium, doping with active ions is a common way to utilize YAG. Er^{3+} has abundant energy levels and at room temperature it can emit lasers of 0.86, 1.64, 1.78, and 2.94 μm when stimulated.

[a] *Multiscale Crystal Materials Research Center, Shenzhen Institute of Advanced Technology, Chinese Academy of Sciences, Shenzhen 518055, China. E-mail: df.xue@siat.ac.cn*
[b] *Institute of Industrial Catalysis, State Key Laboratory Breeding Base of GreenChemical Synthesis Technology, College of Chemical Engineering, Zhejiang University of Technology, Hangzhou 310032, P.R. China*
[c] *State Key Laboratory of Crystal Materials, Institute of Novel Semiconductors, Shandong University, Jinan 250100, China*

† Electronic supplementary information (ESI) available. See DOI: https://doi.org/10.1039/d3ce01081c

The Er^{3+}:YAG solid laser plays an irreplaceable role in ophthalmic surgery. There is a significant difference in the properties of Er^{3+} and Y^{3+} in the YAG melt doped with Er^{3+}, but the segregation coefficient of Er^{3+} in YAG is 1. Besides, as the radius of Er^{3+} is close to that of Y^{3+} and the Er^{3+} valence state is the same as that of Y^{3+},[18,19] other reasons should be more important for the microstructure and dynamics. The influence of doping Er^{3+} on the basic physical properties of YAG melt is a valuable issue in the preparation of Er^{3+}:YAG crystal.

In this work, we researched the Er^{3+}:YAG melt using molecular dynamics simulations. We found that there is a certain equivalence in the structural and dynamics behaviour of Er^{3+} and Y^{3+} in the YAG melt doped with different concentrations of Er^{3+}, which may be one of the reasons why the segregation coefficient of Er^{3+} in YAG is equal to 1. In addition, the relaxation of the network structure, rather than the mass of the ions themselves, affects the diffusion of cations in the melt.

Computational details

In our works, the Buckingham and Coulomb potential model, as shown in the following formula, was used to describe the pair interaction between the ions.

$$U_{ij} = A_{ij}\exp\left(-r/\rho_{ij}\right)\frac{C_{ij}}{r^6} + \frac{q_i q_j}{4\pi\varepsilon r} \quad (1)$$

where r is the distance between the two ions i and j, q_i and q_j are the charges on two ions i and j, respectively, ε is the vacuum dielectric constant, A_{ij}, ρ_{ij}, and C_{ij} are the parameters for the Buckingham potential, as shown in Table 1. Due to the form adopted by the model, there is a characteristic maximum of energy at low r_{max} for the Buckingham model.[20,21] If the distance between the two ions is less than r_{max}, an unphysical attraction will happen. A repulsive term, $V(r_{ij}) = B_{ij}/r^n$ was used to overcome this problem when r is smaller than r', where r' is defined as the r at 0.7 maximum potential energy.[20] Applications for this model, such as the simulation of Y_2O_3 nanoparticles, and Y_2O_3–Al_2O_3 glasses and crystals have shown a good transferability for this model. Furthermore, detailed verification, including crystal elastic constant, lattice constant, radial distribution function, relative proportion among the various coordination units, and bond angle distribution in the melts, was discussed in our previous work about YAG melt,[14] and the model also has a good practicality for describing YAG melts.

Table 1 The parameters of Buckingham potential,[20,21] and repulsive term

Pairs	A (eV)	ρ	C	B (eV)	n
Er–O	58 934.851	0.195478	47.651	469.722	2.714
Y–O	29 526.977	0.211377	50.477	253.661	2.842
Al–O	12 201.417	0.195628	31.997	43.488	3.435
O–O	1844.7458	0.343645	192.58	39.112	3.814

Large-scale Atomic/Molecular Massively Parallel Simulator (LAMMPS)[22] has been used to simulate the YAG melt with periodic boundaries. The Nosé–Hoover method[23,24] was used for canonical (nvt), isothermal-isobaric (npt) ensemble simulation, and the particle–particle algorithm[25] was used to calculate the Coulomb interaction with a precision of 10^{-6}. The time step in all simulations is 1 fs. The pure YAG melt systems include 10 240 ions (the quantity of each kind of ion conforms to the stoichiometric ratio), and the Er^{3+} doping systems were created by replacing Y^{3+} according to nine concentrations of Er^{3+} (3 at%, 6 at%, 9 at%, 12 at%, 15 at%, 20 at%, 30 at%, 40 at%, and 50 at%). Each system was relaxed sufficiently with 500 picoseconds under npt ensemble at temperatures from 2000 to 3200 K with the interval of 200 K, and then simulated under nvt ensemble to collect data for analysis.

Results and discussion

A. Effects on structure

It is necessary to have a clear understanding of the YAG melt structure before discussing the dynamic properties of the melt. YAG melt also belongs to the network-forming systems connected by cationic polyhedra and has an IRO, which has been proved in our previous studies.[14] In most of the metal oxide melts, coordination units (MO_n, M = cations) are formed among the cations, and oxygen ions act as the basic structural unit.[26] Effects of doping Er^{3+} into YAG on the coordination unit between cation-anions (Al–O and Y–O pairs) are inconspicuous. The radial distribution functions (RDF) between the Al and O ions and Y and O ions were calculated using the following formula:

$$g(r) = \frac{V}{N^2}\left\langle \sum_i \sum_{i\neq j} \delta(r - r_{ij}) \right\rangle \quad (2)$$

where V and N represent the system's volume and number of ions, respectively.

The results for 3200 K systems with various concentrations are taken as an example, as shown in Fig. 1. The RDF for pure YAG melt and YAG melt doping Er^{3+} is almost the same. Therefore, doping of Er^{3+} did not change the coordination

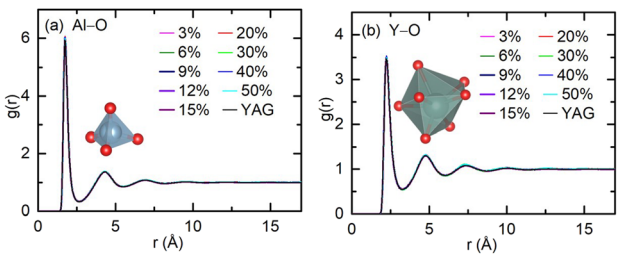

Fig. 1 The RDF for the Al–O (a) and Y–O (b) pairs in the YAG melt (3200 K) with different concentrations (at%) of Er^{3+}. Doping Er^{3+} does not change the coordination units (AlO_n and YO_n shown in insert) in the YAG.

units (AlO_n and YO_n) in YAG. The position (r) corresponding to the first peak in the RDF is the bond length between the two ions. So, the doping concentration also does not change the bond length of the Al–O and Y–O bonds. Although it is difficult to show RDF in all systems with different temperatures, this feature exists for the systems at all temperatures and doping concentrations we simulated, and the RDF between Al–O and Y–O pairs in systems with temperatures of 2000 and 2600 K are shown in Fig. S1 and S2, respectively, in the ESI.†

Er^{3+} doping does not change the relative structure between the ionic coordination units (polyhedrons) in the YAG melts. The RDF between different cation pairs (Al–Al, Y–Y, and Al–Y) were calculated, as shown in Fig. 2. Compared with the RDF for the Al–Al pairs in the pure and Er^{3+}-doped YAG melt, it is clear that the amplitude for each peak and undulating contour for the RDF is not affected by doping, and fluctuations in the longer distance beyond the first peak is also preserved, which means that doping with Er^{3+} did not affect the relative connection between the AlO_n coordination unit, and IRO values are also not affected by Er^{3+}. The situation for the Y–Y and Al–Y cation pairs is similar to that of Al–Al cation pairs. Cations in the melt coordinated with O^{2-} form the polyhedron, these polyhedrons are connected with each other by corner, edge, and face sharing O^{2-}.[14] Doping Er^{3+} into the YAG melt does not impact the connection between cation polyhedrons, and does not enhance or weaken the IRO, which stem from the equivalence between Er^{3+} and Y^{3+}. This feature is not affected by temperature and doping concentrations, and the RDF between Al–Al, Al–Y, and Y–Y pairs in systems with temperatures of 2000 and 2600 K is shown in Fig. S3 and S4, respectively, in the ESI.† The reasons why doping of Er^{3+} does not impact the original network in the melts will be discussed in the next.

The actions of Er^{3+} on the connection between cations units in YAG melt is equivalent to that of Y^{3+}, in other words,

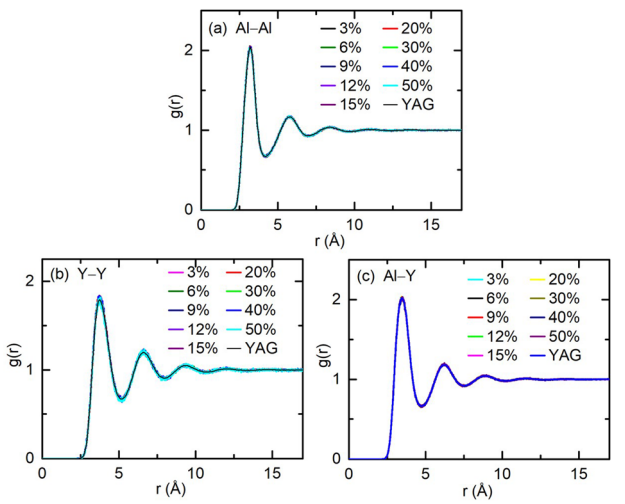

Fig. 2 (a)–(c) respectively represent the RDF between the Al–Al, Y–Y and Al–Y ionic pairs in the YAG (3200 K) with 0, 3, 6, 9, 12, 15, 20, 30, 40, and 50 at% Er^{3+}. The relative structural between the ionic coordination units (polyhedron) in the YAG melts is not affected by doping Er^{3+}.

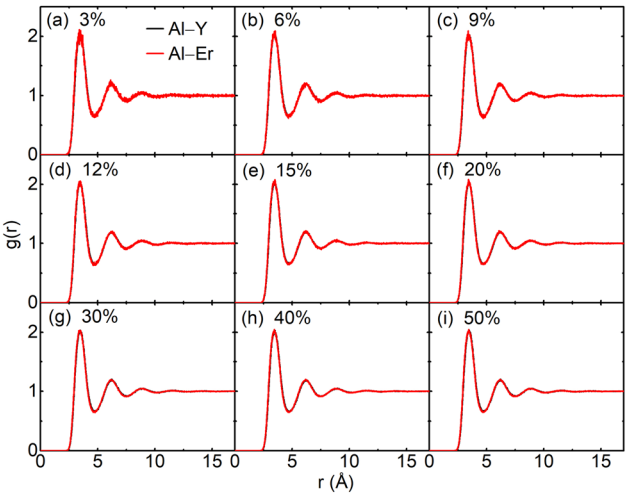

Fig. 3 RDF between Al–Y and Al–Er cation pairs in the melt (3200 K) with 3, 6, 9, 12, 15, 20, 30, 40, and 50 at% doping concentration are showing in (a)–(i) respectively. In terms of Al–Y and Al–Er cation pairs, Er^{3+} is equivalent to the Y^{3+}.

the structural association between Er^{3+} and other cations is the same as that between Y^{3+} and other cations in the Er^{3+}:YAG melts. The RDF between Al–Y, Al–Er, Y–Y, and Y–Er cation pairs was calculated. The results for the systems at 3200 K with various doping concentrations are shown in Fig. 3 and 4. As shown in Fig. 3, RDF for Al–Y and Al–Er pairs are overlapping completely, which indicates that the structural association for Al–Y pairs and Al–Er pairs are equivalent. As shown in Fig. 4, the situation for Y–Y and Y–Er pairs is the same as that with Al–Y and Al–Er pairs. Therefore, in terms of the structural association between Er^{3+} and other cations, Er^{3+} is identical to Y^{3+}, which may result from very little difference between the ionic radii of Er^{3+} (1.004 Å) and Y^{3+} (1.015 Å).[27,28] This equivalence is universal at different

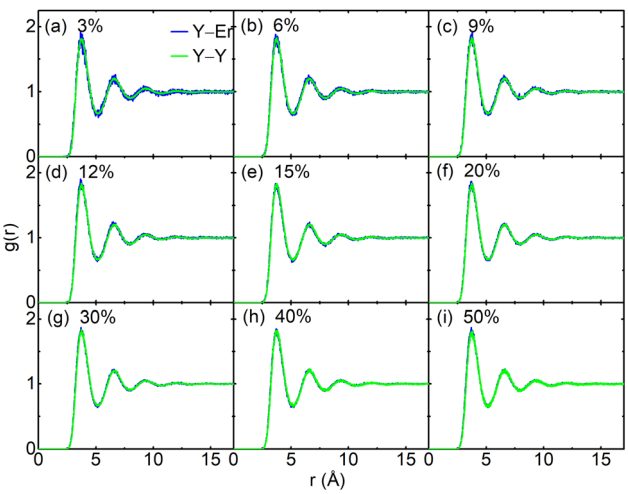

Fig. 4 RDF between the Y–Y and Y–Er cation pairs in the melt (3200 K) with 3, 6, 9, 12, 15, 20, 30, 40, and 50 at% doping concentration are showing in (a)–(i) respectively. In terms of Y–Y and Y–Er cation pairs, Er^{3+} is also equivalent to the Y^{3+}.

temperatures (the RDF between Al–Y, Al–Er, Y–Y, and Y–Er cation pairs in the systems with temperature 2000 and 2600 K is shown in Fig. S5–S8 in the ESI†).

Currently, there are two main reasons for the segregation coefficient of Er^{3+} in YAG to be 1. One is that the ion radius of Er^{3+} is close to that of Y^{3+},[18] and the other is that the valence state of Er^{3+} is the same as that of Y^{3+}.[19] Er^{3+} does not alter the original network structure of YAG, and in the melt structure, Er^{3+} is almost equivalent to Y^{3+}. Therefore, Er^{3+} can completely replace Y^{3+} in any proportion of the melt without changing the melt structure. Segregation is determined by the free energy of the doped ions in crystals and melts. If the difference between Er^{3+} and Y^{3+} in the crystal is ignored, the equivalence of the two ions in the melt has a decisive impact on the segregation coefficient. So, the equivalence between Er^{3+} and Y^{3+} is the fundamental reason why the segregation coefficient of Er^{3+} in YAG is equal to 1.

The equivalence between the Er^{3+} and Y^{3+} is reflected in IRO. The short-range order is different between these two cations, in which the coordination units of Er^{3+} are a little different from that of Y^{3+}. RDF for Er–O and Y–O pairs in the 3200 K systems with various doping concentrations is shown in Fig. 5, and RDF for Er–O and Y–O pairs in the 2000 and 2600 K systems are shown in Fig. S9 and S10, respectively, in the ESI.† Beyond the first peak, RDF for Er–O and Y–O pairs coincided wholly, while the biggest discrepancy occurred in the first peak. The intensity of the first peak in Er–O RDF is greater than that in Y–O RDF, which indicates that the strength of the pair correlation between the Er^{3+} and O^{2-} is stronger than that between Y^{3+} and O^{2-}. The coordination number (CN) for Er^{3+} and Y^{3+} was calculated with the formula, $CN = 4\pi\rho\int_0^{r_{cut}} g(r)r\mathrm{d}r$, where ρ and $g(r)$ are the densities of O^{2-} and RDF, respectively. The coordination numbers for Y^{3+} and Er^{3+} are close to each other in systems with different temperatures and doping concentrations, as shown in Fig. S11(d).† So, the peak intensity of Er–O RDF is higher than that of Y–O RDF, which means that within the coordination structure, the strength of Er–O bond is stronger than that of Y–O, which is the only difference between their local coordination structure. The stronger Er–O bond may be caused by the ion electronegativity for Er^{3+} (1.438), which is greater than that of Y^{3+} (1.340),[29] and the ability for Er^{3+} to attract the negatively charged oxygen ion is stronger than that of Y^{3+}. The entire peak of Er–O RDF tends towards the direction of smaller r, as shown in Fig. S11(a)–(c).† Therefore, the local coordination structure between the Er^{3+} and Y^{3+} is closed, and Er^{3+} slightly has more coordination numbers than Y^{3+} at high temperatures.

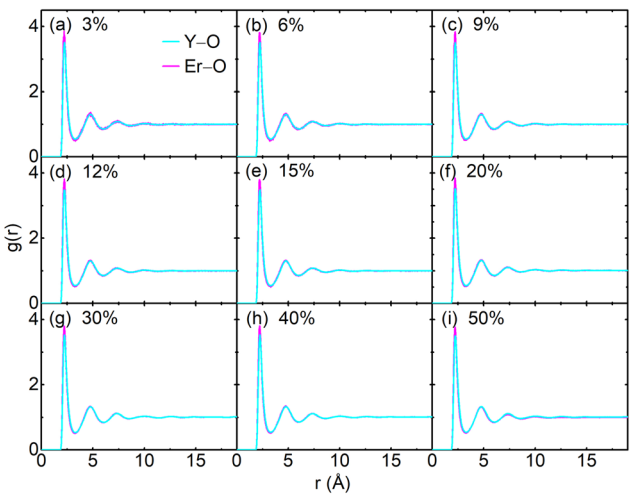

Fig. 5 RDF between Y–O and Er–O cation pairs in the melt (3200 K) with 3, 6, 9, 12, 15, 20, 30, 40, and 50 at% doping concentration are showing in (a)–(i) respectively. Short-range order is obviously different between Er^{3+} and Y^{3+}.

B. Diffusions of ions

In the melt of YAG, the mean squared displacement (MSD) can be divided into three regimes: ballistic, sub-diffusion, and diffusion, which is similar to that of the Al_2O_3 melt.[30] MSD was calculated using the following formula:

$$\mathrm{MSD}(\Delta t) = \langle (r_{t+\Delta t} - r_t)^2 \rangle \quad (3)$$

where r and angle brackets represent the displacement at a certain moment and the ensemble average, respectively.

In the first one, ballistic regime, ions move near the equilibrium position under the action of inertia, as shown in Fig. 6. The moving of ions in this stage belongs to the vibration around the equilibrium position, and the running time is very short (about 100 fs). As shown in Fig. 6(c) and (d), the running times for Er^{3+} and Y^{3+} in the ballistic regime are approximately equal, and this feature is

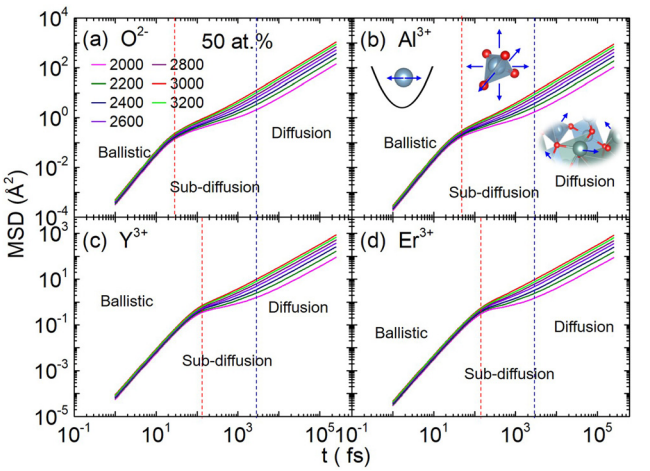

Fig. 6 (a)–(d) respectively represent the function of mean square displacement with time for O^{2-}, Al^{3+}, Y^{3+}, and Er^{3+}, which include three different dynamic stages in Er:YAG (50 at%) melt at different temperature. Additionally, the function of mean square displacement with time in other systems with 3 and 15 at% doping concentration is shown in Fig. S11 and S12.† The mean squared displacement (MSD) can be divided into three regimes: ballistic, sub-diffusion, and diffusion, and the schematic diagram of each stage is shown in the illustration in (b).

not affected by temperature or concentration (MSD for ions in the YAG melts doping with 3 and 15 at% Er^{3+} are shown in Fig. S11 and S12 in the ESI†). If the vibration was treated as a harmonic motion, as shown in the illustration of Fig. 6(b), the running time, $T = 2\pi\sqrt{m/k}$, is proportional to $\sqrt{m}$, where k is related to the stiffness coefficient of the spring and m represents the mass of ions. Therefore, the running time of the Er^{3+} is 1.4 times that of Y^{3+}, which obviously contradicts the current results. Based on the pattern for the coordination structure of cations, the contradictory is attributed to the different coordination environments of Y^{3+} and Er^{3+}. Because Er–O bond is stronger than the Y–O bond, the total interaction between Er^{3+} and O^{2-} is stronger than that between Y^{3+} and O^{2-} (as discussed preceding on the melt structure, other aspects for Er^{3+} and Y^{3+} are equal in the regime beyond the first peak). The stiffness coefficient k for Er^{3+} should be larger than that of Y^{3+}, which can counteract the effect of the mass.

In the second one, sub-diffusive regime, ions move within a local range under the caging effects. Cations in the YAG melt form a coordination structure (polyhedron) with neighbour O^{2-}, and the cations are located inside the polyhedron[14] which is like a cage. The situation for anions is similar, but surrounded by cations. The displacement of ions at this stage mainly stems from the collective movement of the entire cage. Because the entire cage is embedded in the network structure of melts, the displacement is very small, and MSD shows as a plateau. As shown in Fig. 6(c) and (d), the length of the sub-diffusion regime of Y^{3+} and Er^{3+} are the same, which means the dynamic characteristics presented by these two cages corresponding to Y^{3+} and Er^{3+} embedded in the entire network structure are consistent. Additionally, the structural environment of the Y^{3+} and Er^{3+} in the first nearest neighbour is different, while the structural environment outside the first nearest neighbour is consistent. So, it can be inferred that the sub-diffusion behaviours are determined by the structure relaxation beyond the first nearest neighbour.

In the third one, diffusion regime, the imprisoned ions are released by the rearrangement of surrounding ions. The diffusion of ions mainly comes from this stage, and the self-diffusion coefficient is equal to the slope of MSD divided by 6. The relationship between the diffusion coefficient and temperature is shown in Fig. 7. At each doping concentration, the diffusion coefficient of anions is the largest. It is surprising that the diffusion coefficient of the cations is approximately close to each other, but their relative atomic masses are very different (Al: 26.982, Y: 88.906, and Er:167.26). Obviously, the diffusion of cations in these systems is neither determined by the mass of cations nor affected by the coordination unit, because the mass and the coordination unit for each kind of cation is much different.[14] The collaborative rearrangement between the neighbouring cation polyhedrons led to the diffusion of ions. On the one hand, the starting time of diffusion for each kind of ion is basically the same, as shown in the blue dashed line in Fig. 6. On the other hand, the diffusion barrier of cations is also basically the same, as shown in Fig. 8. These two aspects can prove this conjecture. The YAG melt consists of coordination units (AlO_n and YO_n), which are connected with each other by sharing oxygen ions and forming the network structure.[14] Equal barriers for each kind of cation mean the difficulty for rearrangement of the network structure near the cation coordination polyhedron is the same. This indirectly proves that the collaborative relaxation of the medium-range structures affects ion diffusion. On the other side, if the melt structure is divided into two parts, one is the first nearest neighbour and the other is the network structure outside the nearest neighbour, and doping of Er^{3+} only changes the neighbour structure between Er^{3+} and O^{2-}, without affecting the entire networking structures beyond the first neighbour. Doping Er^{3+} into the YAG melt also did not change the diffusion properties of Al^{3+} and Y^{3+}, and the diffusion properties of Er^{3+}

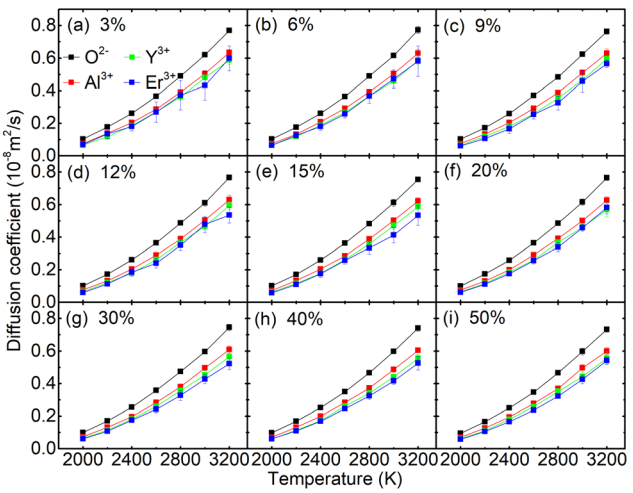

Fig. 7 The relationship between the diffusion coefficient and temperature in the melt with 3, 6, 9, 12, 15, 20, 30, 40, and 50 at% doping concentration are showing in (a)–(i) respectively. The diffusion coefficients of cations are basically equal, which means that ions diffuse in a collaborative form like a cluster.

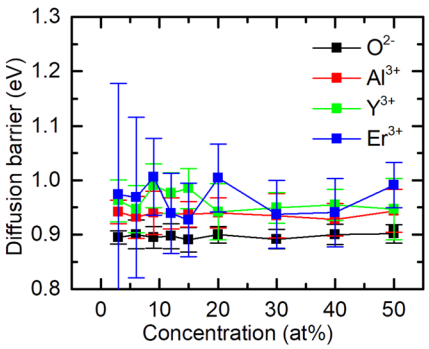

Fig. 8 Relationship between the diffusion barrier and concentration of doping Er^{3+}. The diffusion barrier of cations is approximately equal, which is the reason why the diffusion coefficient for cations is the same. Furthermore, this reflects that the diffusion of cations is carried out through network collaboration rearrangement.

are the same with those of Y^{3+}, which indicate that the diffusion of cations in this kind of network-forming systems is controlled by the collaborative rearrangement of the overall network structure. We speculate that during this rearrangement process, O^{2-} are exchanged between polyhedrons, and the position of the polyhedron changes at the same time, causing all ions to move simultaneously throughout the rearrangement.

Furthermore, the oxide functional crystals play an indispensable role in medical treatment,[31] radiation detection,[32] solid-state laser,[4] and semiconductor fields.[33] However, it is still very difficult to prepare large-sized and high-quality oxide functional crystals.[34] One key reason is that its growth mechanism is not well understood. Crystals are formed by the solidification of atoms transported from liquid to solid by the solid–liquid interface. Although a kinetic mechanism for crystal growth was proposed based on atomic diffusion at the atomic scale,[35–37] this kind of monatomic mechanism has not yet been accurately used to describe the growth process of the complex systems such as oxides.[38] The collaborative rearrangement that happened near the interface may be the main dynamic process. The equivalence between Er^{3+} and Y^{3+} in the melt structure, as well as the unique diffusion behaviour in this system are the possible reasons why Er^{3+} ions only replace the position of Y^{3+} during the crystallization process. Preparation of high-quality Er^{3+}:YAG crystals will promote the application of solid-state lasers.[39–41]

Conclusions

Although the properties of Er^{3+} are significantly different from those of Al^{3+} and Y^{3+}, the effect of E^{3+} doping on the melt structure in YAG melt is localized in the first nearest neighbour of the coordination structure between Er^{3+} and O^{2-}, and doping Er^{3+} does not change the original network-forming structure characteristics between the cations. The localization effect for doping Er^{3+} is independent of the doping concentration and the temperature of the systems. The diffusion coefficients of different ions are almost the same in each system with different doping concentrations of Er^{3+} and different temperatures above or near melting points. Real diffusion of ions in the Er^{3+}:YAG melt is caused by the overall collaborative rearrangement of the overall structure in the network-forming systems. In terms of the structure and dynamics properties, Er^{3+} is equivalent to Y^{3+} in the YAG melt at different temperatures and doping concentrations, which may be the microscopic reason for the segregation coefficient of Er^{3+} to be 1 in YAG.

Conflicts of interest

There are no conflicts to declare.

Acknowledgements

This project was supported by the National Natural Science Foundation of China for Youth (52202012), Key projects of the National Natural Science Foundation of China (51832007), International (regional) cooperation and exchange projects (52220105010), 2021 Sino-German Cooperation and Exchange Program of the Sino-German Science Center of the National Natural Science Foundation (M-0755), Major basic research project of Shandong Natural Science Foundation (ZR2020ZD35).

References

1 A. M. Hofmeister and K. R. Campbell, *J. Appl. Phys.*, 1992, **72**(2), 638–646.
2 R. D. Shannon, M. A. Subramanian and T. H. Allik, *et al.*, *J. Appl. Phys.*, 1990, **67**(8), 3798–3802.
3 P. R. Stoddart, P. E. Ngoepe and P. M. Mjwara, *et al.*, *J. Appl. Phys.*, 1993, **73**(11), 7298–7301.
4 B. Ma, W. Zhang and H. Luo, *et al.*, *Opt. Mater.*, 2023, **143**, 114218.
5 L. Lv, J. He and Q. Xiao, *et al.*, *Ceram. Int.*, 2023, **49**(17, Part A), 28457–28464.
6 V. Laguta, M. Buryi and V. Babin, *et al.*, *J. Mater. Chem. C*, 2023, **11**(4), 1346–1359.
7 J. K. R. Weber, S. Krishnan and S. Ansell, *et al.*, *Phys. Rev. Lett.*, 2000, **84**(16), 3622–3625.
8 B. R. Johnson and W. M. Kriven, *J. Mater. Res.*, 2001, **16**(6), 1795–1805.
9 K. Nagashio, J. Sasaki and K. Kuribayashi, *Mater. Trans.*, 2004, **45**(8), 2723–2727.
10 M. Wilson and P. F. McMillan, *Phys. Rev. B: Condens. Matter Mater. Phys.*, 2004, **69**(5), 054206.
11 V. Cristiglio, L. Hennet and G. J. Cuello, *et al.*, *J. Phys.: Condens. Matter*, 2007, **19**(41), 415105.
12 L. Hennet, S. Krishnan and I. Pozdnyakova, *et al.*, *Pure Appl. Chem.*, 2007, **79**(10), 1643–1652.
13 V. Cristiglio, L. Hennet and G. J. Cuello, *et al.*, *J. Non-Cryst. Solids*, 2007, **353**(18–21), 1789–1792.
14 X. Zhang, F. Liu and K. Chen, *et al.*, *CrystEngComm*, 2023, **25**(16), 2410–2417.
15 M. C. Wilding, M. Wilson and P. F. McMillan, *Philos. Trans. R. Soc. London*, 2005, **363**(1827), 589–607.
16 G. N. Greaves, M. C. Wilding and D. Langstaff, *et al.*, *J. Non-Cryst. Solids*, 2011, **357**(2), 435–441.
17 P. F. McMillan, M. Wilson and M. C. Wilding, *et al.*, *J. Phys.: Condens. Matter*, 2007, **19**(41), 415101.
18 D. Zhou, X. Xu and C. Xia, *et al.*, *J. Opt. Soc. Am. B*, 2011, **28**(10), 2543–2548.
19 S. Bera, P. Ohodnicki and K. Collins, *et al.*, *J. Cryst. Growth*, 2020, **547**, 125801.
20 J. Du and A. N. Cormack, *J. Non-Cryst. Solids*, 2005, **351**(27), 2263–2276.
21 J. C. Du, *J. Am. Ceram. Soc.*, 2009, **92**(1), 87–95.
22 S. Plimpton, *J. Comput. Phys.*, 1995, **117**(1), 1–19.
23 W. G. Hoover, A. J. C. Ladd and B. Moran, *Phys. Rev. Lett.*, 1982, **48**(26), 1818–1820.
24 S. Nosé, *Mol. Phys.*, 1984, **52**(2), 255–268.
25 J. W. Eastwood, R. W. Hockney and D. Lawrence, *Comput. Phys. Commun.*, 1980, **19**(2), 215–261.
26 L. B. Skinner, C. J. Benmore and J. K. R. Weber, *et al.*, *Phys. Rev. Lett.*, 2014, **112**(15), 157801.

27 J. Kimpton, T. H. Randle and J. Drennan, *Solid State Ionics*, 2002, **149**(1), 89–98.
28 Y. Q. Jia, *J. Solid State Chem.*, 1991, **95**(1), 184–187.
29 K. Li and D. Xue, *J. Phys. Chem. A*, 2006, **110**(39), 11332–11337.
30 N. T. T. Ha, N. V. Hong and P. K. Hung, *Indian J. Phys.*, 2019, **93**(8), 971–978.
31 T. C. D. Carrieri, P. M. de Freitas and R. S. Navarro, *et al.*, *Lasers Med. Sci.*, 2007, **22**(3), 165–170.
32 Z. Luchuan, X. Chao and C. Yongkang, *et al.*, Luminescence and Scintillation Characteristics of Lyso:Ce Dosimeter for Low Dose X-Ray, *Proc. SPIE*, 2022, 123210R.
33 C. J. Ou, K. P. Chang and M. W. Tasi, *et al.*, *IEEE Photonics J.*, 2022, **14**(6), 1–9.
34 F. Liu, K. Chen and D. Xue, *Innovation*, 2023, **4**(4), 100458.
35 J. Q. Broughton, G. H. Gilmer and K. A. Jackson, *Phys. Rev. Lett.*, 1982, **49**(20), 1496.
36 G. Sun, J. Xu and P. Harrowell, *Nat. Mater.*, 2018, **17**(10), 881–886.
37 Q. Gao, J. D. Ai and S. X. Tang, *et al.*, *Nat. Mater.*, 2021, **20**(10), 1431–1439.
38 F. Liu, K. Chen and C. Peng, *et al.*, *J. Appl. Phys.*, 2023, **133**(17), 175301.
39 X. Zang, Z. Liu and Y. Xu, *et al.*, *Sci. China: Technol. Sci.*, 2023, **66**, DOI: **10.1007/s11431-023-2420-x**.
40 G. Zhao, G. Wang and Y. Li, *et al.*, *Sci. China: Technol. Sci.*, 2023, **66**, DOI: **10.1007/s11431-022-2327-8**.
41 J. Tan, Y. Lyu and J. Zhang, *et al.*, *Sci. China: Technol. Sci.*, 2023, **66**, 3439–3449.